NANO LETTERS

ACS EDITORS' CHOICE

pubs.acs.org/NanoLett

Letter

Plasmonic and Electrostatic Interactions Enable Uniformly Enhanced Liquid Bacterial Surface-Enhanced Raman Scattering (SERS)

Loza F. Tadesse,* Chi-Sing Ho, Dong-Hua Chen, Hamed Arami, Niaz Banaei, Sanjiv S. Gambhir, Stefanie S. Jeffrey, Amr A. E. Saleh,* and Jennifer Dionne*

Cite This: *Nano Lett.* 2020, 20, 7655−7661

Read Online

ACCESS | Metrics & More | Article Recommendations | Supporting Information

ABSTRACT: Surface-enhanced Raman spectroscopy (SERS) is a promising cellular identification and drug susceptibility testing platform, provided it can be performed in a controlled liquid environment that maintains cell viability. We investigate bacterial liquid-SERS, studying plasmonic and electrostatic interactions between gold nanorods and bacteria that enable uniformly enhanced SERS. We synthesize five nanorod sizes with longitudinal plasmon resonances ranging from 670 to 860 nm and characterize SERS signatures of Gram-negative *Escherichia coli* and *Serratia marcescens* and Gram-positive *Staphylococcus aureus* and *Staphylococcus epidermidis* bacteria in water. Varying the concentration of bacteria and nanorods, we achieve large-area SERS enhancement that is independent of nanorod resonance and bacteria type; however, bacteria with higher surface charge density exhibit significantly higher SERS signal. Using cryo-electron microscopy and zeta potential measurements, we show that the higher signal results from attraction between positively charged nanorods and negatively charged bacteria. Our robust liquid-SERS measurements provide a foundation for bacterial identification and drug testing in biological fluids.

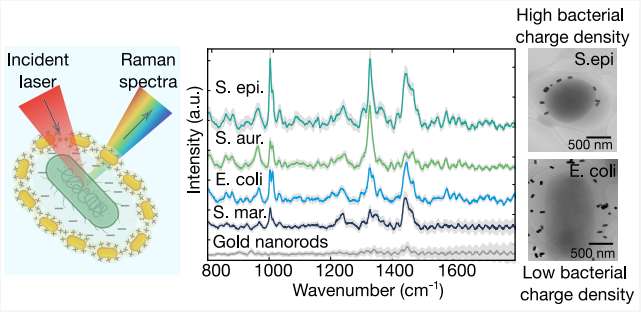

KEYWORDS: *surface-enhanced Raman spectroscopy (SERS), infectious disease, gold nanorods, bacteria, cryo-electron microscopy*

Rapid bacterial detection, identification, and antibiotic susceptibility testing is a critical clinical challenge. Standard bacterial diagnostics requires culturing steps that are naturally slow, accompanied by separate identification and antibiotic susceptibility tests that together span several days.[1] Molecular diagnostic tools such as polymerase chain reaction (PCR),[2] matrix-assisted laser desorption/ionization time-of-flight mass spectrometry (MALDI-TOF),[3] and lateral flow enzyme immunoassays (EIA)[4,5] can expedite the process but still require hundreds of thousands of cells, significant capital investment, and/or cell-specific labels for high-fidelity testing; they are also destructive tests and hence are ill-suited for real-time drug susceptibility testing.

Vibrational spectroscopy-based approaches such as Raman and Infrared spectroscopy promise culture-free, label-free, fast, accurate, and sensitive identification of bacteria with minimal sample preparation and without significant cell damage.[6−11] These techniques provide a spectroscopic fingerprint of bacterial cells, with signal enhancements afforded by plasmonic substrates via either surface-enhanced Raman spectroscopy (SERS) or infrared absorption spectroscopy (SEIRA).[12−15] For portable, low-cost diagnostics, SERS has gained particular traction: the visible-frequency excitation and detection of SERS allows single-cell-level[16] sensitivity as well as cheaper detectors and light sources. Further, its integration with microfluidics[17−19] along with the development of paper-based SERS assays[20] and portable Raman microscopes[21] increases its accessibility for clinical application.[22] Still, although considerable advances in the field of bacteria identification with SERS have been shown, many studies to date use dried samples because of the ease of sample preparation and spectral acquisition.[17,23] In contrast, clinical samples are generally in the liquid state, as drying can be detrimental to the cells, removes or modifies important biological information from the SERS spectra, and does not allow dynamic study on the effect of antibiotics on bacterial cells.

Although clinically desirable, liquid Raman measurements present several challenges. Scattering from the inhomogeneous bacterial liquid with variations in dielectric constants leads to signal loss. Liquid SERS also requires devising easy-to-use and safe (i.e., free of hazardous bacterial exposure) platforms with optically compatible components. Efforts have been made to enable SERS measurements from liquid droplets on sub-

Received: August 3, 2020
Revised: September 10, 2020
Published: September 11, 2020

strates.[24−26] However, the droplets were open to air, increasing the risk of aerosol/droplet exposure to the individuals performing measurements on pathogenic bacteria. Additionally, droplets tend to dry over a period of minutes, possibly providing insufficient interrogation time for bacteria identification and especially antibiotic susceptibility testing. This approach also limits the number of cells that can be analyzed to the size of the droplet. Microfluidic approaches[18,27−32] have gained traction in advancing liquid SERS; here, the flow rate even at the single-cell level can be synchronized with the Raman signal acquisition for achieving targeted cell sorting, as demonstrated in yeast strains *Saccharomyces cerevisiae*.[33] This approach, however, can only handle small sample volumes. Additionally, the strong Raman background from the commonly used PDMS material interferes with weak Raman signals from smaller cell types like bacteria compared to yeast. Moreover, for all existing liquid SERS approaches, there remains the need to understand and optimize plasmonic particle and bacterial cell interaction for efficient, uniform SERS enhancement.

Here we demonstrate a liquid bacterial SERS platform with consistent, large-area SERS enhancement. In particular, we investigate the effects of bacterial surface charge, the gold−nanorod aspect ratio, and nanoparticle concentration to systematically determine the optimal parameters for liquid SERS. We use Gram-negative *E. coli* and *S. marcescens* and Gram-positive *S. aureus* and *S. epidermidis* as model bacteria to study their interaction with gold nanorods. By optimizing the nanorod to bacteria concentration ratios, we obtain SERS signatures from liquid bacteria samples with signal intensities uniformly enhanced to detectable levels (compared to no signal with bacteria in water) across a 100 × 200 μm^2 area. Interestingly, the enhancement does not significantly vary with distinct nanorod aspect ratios, regardless of overlap with the laser excitation and Raman region of the bacteria; however, Gram-positive bacteria do show more significant enhancement. Cryo-electron microscopy (cryo-EM) reveals variations in nanoparticle binding affinities to Gram-positive and -negative bacterial types, depending on the charge of the bacteria membrane. As such, the bacteria with higher surface charge density also exhibit significantly higher SERS signal. Our work lays a foundation for performing, optimizing, and understanding liquid SERS measurements from biological fluids en route to clinical SERS and real-time drug susceptibility testing.

We created a liquid chamber (hereafter "well") for live bacterial SERS measurements as shown in Figure 1a. The well consists of a silicon wafer base, ∼100 μm tall spacer layer, and glass coverslip; double-sided adhesive was used for the spacer layer, punched using single paper hole punchers to create reproducible liquid well sizes. The liquid bacterial sample is pipetted into the well, then sealed with a coverslip and placed on a microscope stage for SERS imaging. Gold nanorods with longitudinal plasmon resonances ranging from 670−860 nm, governed by their aspect ratio, were colloidally synthesized via a seeded growth: reduction of $HAuCl_4$ with sodium borohydride creates a spherical seed solution. The seed solution and additional gold salt is mixed with $AgNO_3$, HCl, ascorbic acid, hexadecyl(trimethyl)ammonium bromide (CTAB), and sodium oleate for nanorod formation (see Figure S1). The target aspect ratio is controlled by the concentrations of each agent, as described in the literature.[34] All nanorods are coated with sodium oleate and CTAB, giving them a slightly positive charge, as confirmed by zeta potential

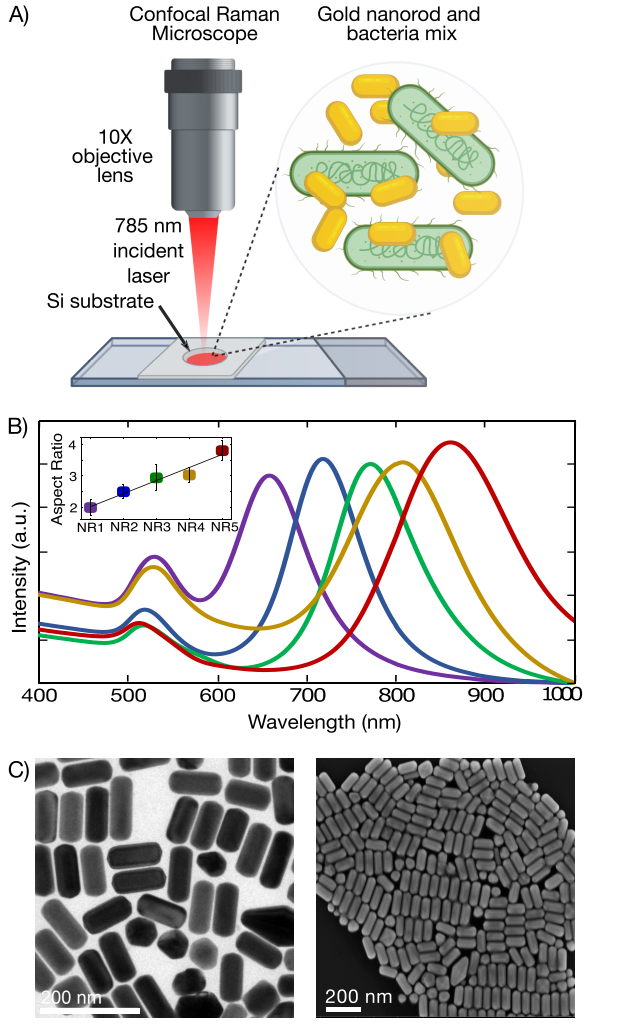

Figure 1. Overview of liquid-SERS chamber and plasmonic nanoparticles employed. (A) Liquid well imaging setup with bacteria (green) and nanorods (gold) both suspended in water and mixed together in the well. The well is fabricated using a Si wafer base and a double-sided adhesive spacing layer and sealed with a coverslip (see also Figure S15). (B) Absorption spectra of nanorods in the liquid well with longitudinal plasmon resonances ranging from 670−860 nm. Inset shows aspect ratios plotted against peak resonance wavelength. The dashed line indicates the 785 nm incident laser used for measurement. The region from ∼835−915 nm (annotated with redline) represents the bacterial Raman shift region. (C) TEM (left) and SEM (right) of synthesized gold nanorod particles used for liquid SERS measurement, showing monodispersity in nanorod size and shape. Additional images are included in Figure S1.

measurements (see the Figure S11). UV−vis absorption spectra (Figure 1b) and transmission and scanning electron micrographs (TEM and SEM) of the gold nanorod samples (Figure 1c) confirm the red-shifting of the longitudinal plasmon resonance peak with increasing aspect ratio.

We varied the bacteria and Au nanorod mixing ratio and preparation conditions to obtain maximally enhanced SERS signatures while keeping the bacteria viable. Importantly, because the CTAB surfactant from the gold nanorods is cytotoxic, we tested the number of water washing steps needed for aggregation-free nanoparticle dispersion with minimal surfactant coverage to preserve bacterial cell viability. Figures S2 and S3 include bacterial growth/viability tests following mixing with nanorods (NRs) that are not purified with water

https://dx.doi.org/10.1021/acs.nanolett.0c03189
Nano Lett. 2020, 20, 7655−7661

and purified with water at 1, 2, and 3× washing. We find that cell viability is maintained with one washing step, as evidenced by cell growth; additional washing steps lead to comparable bacterial viability but significant nanorod aggregation. We also investigated the concentration of nanorods to bacteria, spanning 10, 30, 50, and 100% (double volume of nanorod to bacteria) volumetric ratios. As shown in Figure S2 and Table S2, all ratios maintain cell viability and show significant SERS, with the highest signal generally observed for the largest ratio. Hence, a 1:1 volumetric ratio (5 μL of 1×10^9 cells/mL bacteria with 5 μL of NR) is used for ease of experimental workflow.

Using a 785 nm laser, we obtained strongly enhanced SERS signatures from the liquid wells with bacteria and nanorods compared to bacteria-only samples. All measurements are obtained using a 5×, 0.12NA objective lens with a 30 μm focal spot and experimental conditions chosen to maximize translation to point-of-care clinical applications (i.e., portable, low-cost systems). Figure 2a includes representative SERS spectra from *E. coli* suspended in water ($\sim 1 \times 10^9$ cells/mL, from log-phase of bacteria culture) showing the significant Raman signal enhancement achieved in liquid samples when mixed with nanorods compared to *E. coli* only. Figure 2b shows the average spectra, each collected with 10 s acquisition time, from the four bacterial species *E. coli*, *S. marcescens*, *S. aureus* and *S. epidermidis*, respectively. With the 670 nm resonant nanorods, bacterial signature spectral peaks near 1000, 1350, and 1500 cm^{-1} are observed. The liquid-SERS signatures are nearly identical with the SERS signatures seen with dried specimens;[23] we note that in both dried and liquid cases, the SERS results from a combination of cellular structures (membrane proteins, lipids, and intracellular components) as well as excreted metabolites (including metabolites resulting from stress responses to nutrient-poor aqueous media, as in our well).[19] As Figure 2a, b shows, spectra from the samples without nanorods have no signal under the same interrogation settings; hence detectable spectra are attributed to enhancement from nanorods (see Figure S4).

Next, we collected SERS spectra across a 100×200 μm^2 region within our liquid well. Again, using our 670 nm resonant nanorods, we obtain uniform Raman signal enhancement for each of the four bacteria, as shown in Figure 2c and Figure S5. Importantly, the peak signals vary by ~25% across the entire scanned area, which is reasonable given the size of the area scanned and the large spot size of 30 μm. We also tested the well-to-well reproducibility by using *S. epidermidis* mixed with our 860 nm resonant nanorods. As seen in Figure S6, each liquid well shows comparable spectral enhancement with the mean of measurements across the 100×200 μm^2 area across five separate wells with a variation of ~15%.

We explored how each nanorod with specific longitudinal plasmon resonance peaks enhances the liquid SERS signals. We considered the five NRs of Figure 1b and constructed 30 distinct liquid wells, each containing 1:1 bacteria:NR volumetric ratio mixtures. These NR aspect ratios are chosen such that their peak plasmon resonance wavelength spans the relevant optical ranges for SERS including incident illumination (785 nm) and the bacterial Raman shift region (~835–915 nm). As seen in Figure 3, all NR samples show strong SERS signatures. Interestingly, the NR-to-NR variability in signal is comparable to the well-to-well signal variability (see Figure S6) for a given aspect ratio and bacteria sample.

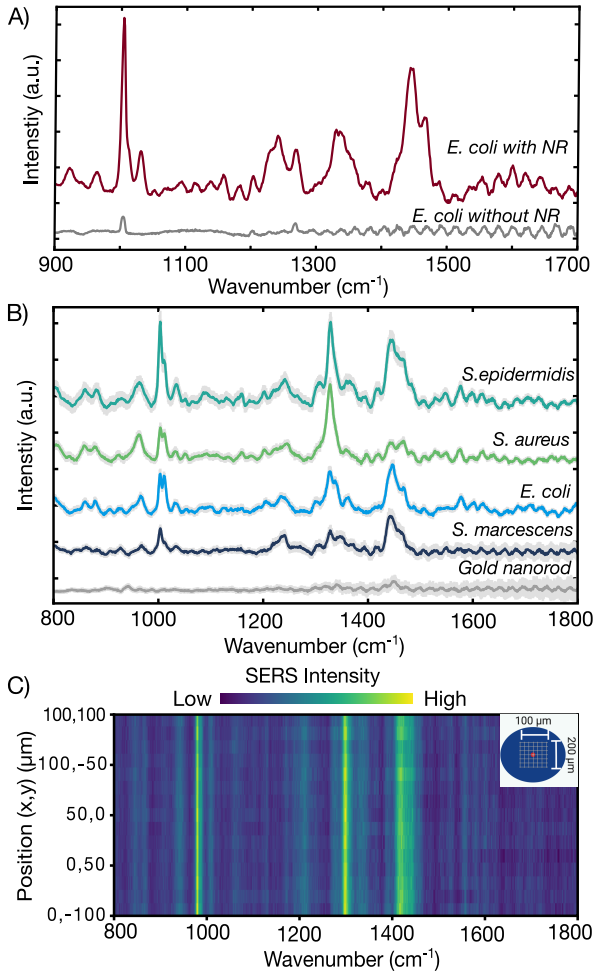

Figure 2. Spectral enhancement consistency across a large surface area of the well and among multiple liquid-SERS chambers. (A) Comparison of *E. coli* Raman spectra with and without the 670 nm nanorods, acquired at 60 s with 5 accumulation, showing no significant spectral signature from liquid *E. coli* samples without nanorods. (B) Liquid-SERS spectra of the four bacterial species mixed with the 670 nm nanorods with the average and standard deviation of 15 measurements at 10 s acquisition across 100×200 μm^2 dimension on the well (inset in C). (C) Heatmap plot of the *S. epidermidis* spectra shown in B highlighting the consistency of enhancements across the large area. Each row is a spectrum recorded from unique locations on the well. The inset is a schematic showing the *xy* map region scanned on the liquid well.

Therefore, within the error of these measurements, all NRs show strong enhancement.

The lack of trend in enhancement factor with NR aspect ratio (peak plasmon resonance) counters standard intuition from dried SERS measurements. In liquids, the nanorods are fairly uniformly distributed throughout the liquid volume. Hence, both incident and scattered light strongly interact with the nanorods as light travels across the liquid volume beyond the measurement plane. This interaction becomes particularly strong when the nanorod resonance overlaps with either the excitation wavelength or the bacteria Raman scattering wavelengths. Accordingly, a "competition between extinction and enhancement" effect as described by van Dijk et al. and Sivapalan et al.[35,36] arises, compromising the expected higher enhancement at these wavelengths. On the contrary, when the NR resonance is blue-shifted away from these regions of strong

https://dx.doi.org/10.1021/acs.nanolett.0c03189
Nano Lett. 2020, 20, 7655−7661

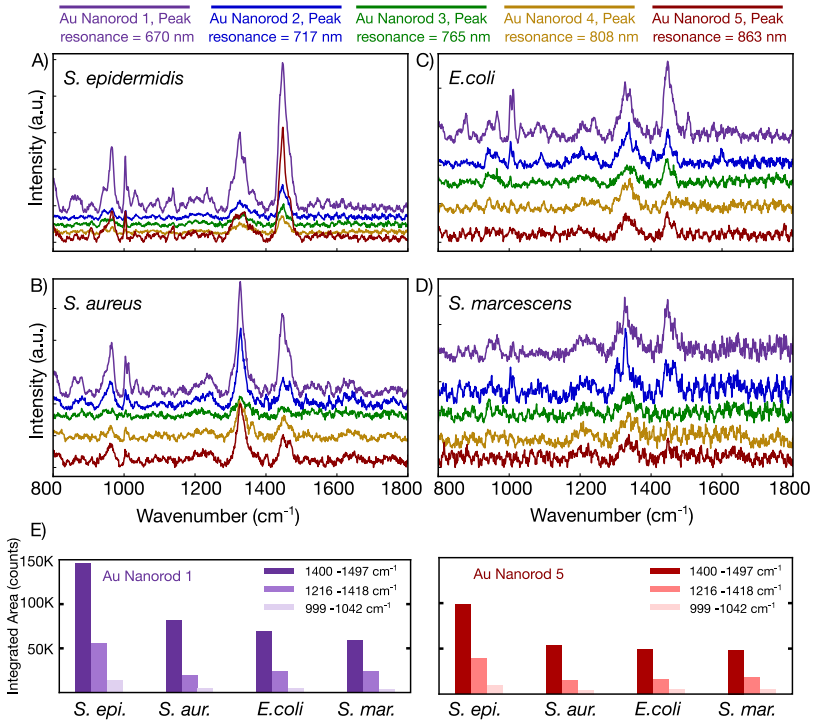

Figure 3. SERS spectra comparison across nanorods and bacteria. (A) *S. epidermidis* spectra combined with the five NRs, color coded and arranged such that the most blue-shifted is on top and most red-shifted at the bottom. (B) *S. aureus*, (C) *E. coli*, and (D) *S. marcescens* SERS spectra when mixed with the five nanorods tested. (E) Area under the peak values for signature bacterial peaks near 1000, 1300, and 1500 cm^{-1} showing higher values for *S. epidermidis* and *S. aureus*, which have higher negative surface charge compared to *E. coli* and *S. marcescens*. The bar plots shown are for the 670 and 863 nm resonant nanorods (see Figure S9.

competition, the overall setup shows a relatively higher enhancement profile.

Interestingly, higher counts are observed for the NR with the lowest aspect ratio, most blue-shifted from the laser excitation (see Figure S7). Such enhancements have also been corroborated by other liquid-SERS studies on trap-coated methylene blue molecules and attributed to reduced extinction effects. As discussed above, when using nanorods with resonances matched to the incident laser or the Raman region, both the laser and the Raman scattered light are absorbed by the nanoparticles themselves before reaching the bacterial cells and the detector, respectively. However, when using blue-shifted nanorods, these extinction effects are avoided.[35,36] Still, within the variability of multiple measurements from distinct wells, we have not observed a statistically significant difference for SERS from rods of any size. In addition, it can be seen from Figure 3 that the most red-shifted nanorods still contribute to signal enhancement significantly in *S. epidermidis* and *S. aureus* cases. Our results indicate that all nanorod aspect ratios provide significant enhancement for recording SERS signatures from liquid bacterial samples compared to bacteria-only samples suspended in water (see Figure S4).

Gram-positive and highly negatively charged *S. epidermidis* and *S. aureus* overall show more distinct, higher intensity spectra than the Gram-negative *E. coli and S. marcescens* species. Specifically, *S. marcescens* shows consistent reduced spectral signal intensity across the nanorods tested and multiple trials while *E. coli* tends to be lower or comparable in repeat studies (see Figure S8). In our study the selected Gram-negative species harbor lower negative surface charge, with *E. coli* and *S. marcescens* having negative surface charge densities of ∼0.01 and ∼0.04 (r/e (−)/(1 × 10^{-6}) mm^2), respectively, whereas the Gram-positive *S. epidermidis* and *S. aureus* have negative surface charge densities of ∼1 and ∼0.3 (r/e (−)/(1 × 10^{-6}) mm^2). *S. epidermidis,* in particular, has nearly two orders of magnitude higher negative charge density which could significantly contribute to stronger electrostatic interactions with the positively charged nanorods (see also Table S1). Figure 3e illustrates the higher enhancement observed in higher surface charge harboring species. We plot the integrated intensity for spectral peaks near 1000, 1300, and 1500 cm^{-1} wavenumbers for two sets of nanorods (additional nanorod SERS data is in Figure S9). Across all nanorods, significantly higher SERS signal is observed for *S. epidermidis* and *S. aureus*, which have higher negative surface charge compared to *E. coli* and *S. marcescens.*

To better understand the local interaction between the cells and NRs in our liquid well, we performed cryo-EM. We froze our liquid bacteria−NR mixture onto a 200-mesh Cu lacey carbon grid to image the nanorod distribution on the bacteria as-is in liquid (see Figure S10 of dried SEM images). We imaged with a low dose at −177 °C. The cryo-EM images show distinct differences in the arrangement of NRs around Gram-negative and Gram-positive bacteria. As seen in Figure 4, the NRs surround Gram-positive *S. epidermidis* by closely binding to its membrane surface, whereas in the case of Gram-negative *E. coli,* the nanorods do not show specific adherence to the bacterial membrane surface. The observed close binding is because of the positive surface charge of the NRs (resulting from the CTAB surfactant on their surface, confirmed by the zeta-potential measurements shown on Figure S11) interacting with the negative surface charge on the bacterial membrane. In particular, *S. epidermidis* has ∼30× higher negative charge with significantly smaller surface area compared to *E. coli* (see Table

https://dx.doi.org/10.1021/acs.nanolett.0c03189
Nano Lett. 2020, 20, 7655−7661

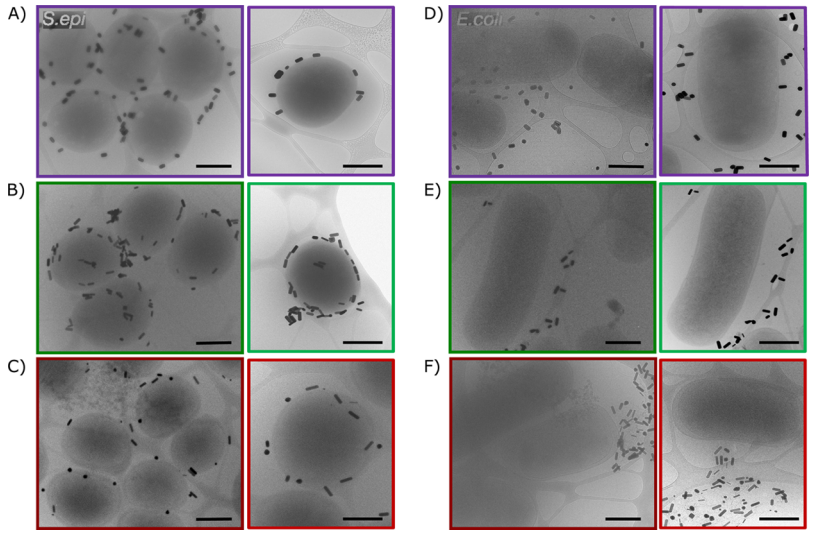

Figure 4. Interaction between bacterial cells and nanoparticles and its effect on Raman signal enhancement. Cryo-EM images of *S. epidermidis* (left column) mixed with three NRs with longitudinal plasmon resonance peaks and color coding: (A) 670 nm, purple; (B) 717 nm, green; and (C) 860 nm, red, respectively. Similarly, *E. coli* (right column) mixed with three NRs with longitudinal plasmon resonance peaks and color coding: (D) 670 nm, purple; (E) 717 nm, green; and (F) 860 nm, red, respectively. The nanoparticles show tight binding to *S. epidermidis* cell surface compared to *E. coli* cell surfaces, as the former has a higher negative surface charge. Scale bar indicates 500 nm.

S1). The large charge distributed over a small surface area allows *S. epidermidis* to have nearly two orders of magnitude higher charge density than *E. coli,* resulting in a stronger electrostatic interaction with the positively charged NRs.

We also confirmed no significant change in the full-width half max and plasmon peak location (there is a slight red shift with addition of bacteria which can be attributed to the slight increase in refractive index of the solution) of the nanorods when mixed with the bacteria species (see supplemental Figure 12). Interestingly, the spectral data from three isolated trials comparing the SERS enhancement for *S. epidermidis* and *E. coli* do not show statistically significant differences upon repeated measurements as shown in Figure S13. Therefore, although differences in surface charge lead to different NR coverage on individual bacterial cells and thus variations in enhancement, the NRs still effectively enhance the overall SERS signal as the NRs and cells can freely interact in the dynamic liquid environment. Furthermore, bacterial NR mixtures were measured within a few minutes, after 5 h, and after 24 h and were tested and show new peaks arising near 1600 cm^{-1} with time (24 h), which can be attributed to cellular death showing the potential use of such liquid wells for monitoring live cell changes across time, see Figure S14.

In summary, we have demonstrated a simple and robust liquid Raman well setup that enables uniform, large-area SERS enhancement of bacteria in liquid while maintaining cell viability and prevents exposure to pathogenic bacteria under investigation. Our results show that bacteria with higher negative surface charge better attract the positively charged Au NRs, leading to higher SERS enhancements. Furthermore, several NRs with longitudinal plasmon resonance peaks ranging from 670 to 870 nm can be used to obtain SERS enhancements despite the differences in peak location.

Our work could facilitate clinical translation of Raman-based diagnostics. For example, in the realm of antibiotic testing, combination therapy is gaining traction as a more effective treatment approach compared to single antibiotic treatments;[37] a reliable liquid-SERS environment integrated with inflow and outflow channels could be used to test the effect of combined antibiotic therapy on pathogens by monitoring dynamic changes in the bacteria directly from Raman spectral changes. Liquid-SERS could also enable real-time drug susceptibility testing on cancer cells, without the need for fixing or freezing of the cells, potentially at the single-cell level. Additionally, liquid SERS could enable viable bacterial identification at low concentrations, which is especially important for bacteria that are difficult to culture, such as in microbiome studies and environmental microbiology.[38] Lastly, in pharmaceutical applications such as drug discovery, liquid-SERS could be used to monitor chemical composition of excreted factors in combined cultures while maintaining cellular viability.[39,40] Our simple sample preparation platform and rigorous understanding of liquid bacterial SERS hopefully provides a foundation for such studies and more en route to low-cost point-of-care diagnostics.

■ ASSOCIATED CONTENT

Supporting Information

The Supporting Information is available free of charge at https://pubs.acs.org/doi/10.1021/acs.nanolett.0c03189.

Materials and Methods, Figures S1−S15, and Tables S1 and S2 (PDF)

■ AUTHOR INFORMATION

Corresponding Authors

Loza F. Tadesse − *Department of Bioengineering, Stanford University School of Medicine and School of Engineering, Stanford, California 94305, United States;* orcid.org/0000-0003-2040-8145; Email: lozat@stanford.edu

Amr A. E. Saleh − *Department of Materials Science and Engineering, Stanford University School of Engineering, Stanford, California 94305, United States; Department of Engineering Mathematics and Physics, Faculty of Engineering, Cairo University, Giza 12613, Egypt;* orcid.org/0000-0001-7136-3683; Email: aessawi@stanford.edu

https://dx.doi.org/10.1021/acs.nanolett.0c03189
Nano Lett. 2020, 20, 7655−7661

Jennifer Dionne − *Department of Materials Science and Engineering, Stanford University School of Engineering, Stanford, California 94305, United States; Department of Radiology, Molecular Imaging Program at Stanford (MIPS) Stanford University School of Medicine, Stanford, California 94305, United States;* orcid.org/0000-0001-5287-4357; Email: jdionne@stanford.edu

Authors

Chi-Sing Ho − *Department of Applied Physics, Stanford University, Stanford, California 94305, United States; Department of Materials Science and Engineering, Stanford University School of Engineering, Stanford, California 94305, United States*

Dong-Hua Chen − *Department of Structural Biology, Stanford University, Stanford, California 94305, United States*

Hamed Arami − *Department of Radiology, Molecular Imaging Program at Stanford (MIPS)Stanford University School of Medicine, Stanford, California 94305, United States*

Niaz Banaei − *Department of Pathology, Stanford University School of Medicine, Stanford, California 94305, United States; Clinical Microbiology Laboratory, Stanford Health Care, Stanford, California 94305, United States; Department of Infectious Diseases and Geographic Medicine, Stanford University, Stanford, California 94305, United States*

Sanjiv S. Gambhir − *Department of Bioengineering, Stanford University School of Medicine and School of Engineering, Stanford, California 94305, United States; Department of Materials Science and Engineering, Stanford University School of Engineering, Stanford, California 94305, United States; Department of Radiology, Molecular Imaging Program at Stanford (MIPS)Stanford University School of Medicine, Stanford, California 94305, United States; Stanford Neuroscience Institute, Stanford University, Stanford, California 94305, United States;* orcid.org/0000-0002-2711-7554

Stefanie S. Jeffrey − *Department of Surgery, Stanford University School of Medicine, Stanford, California 94305, United States;* orcid.org/0000-0003-4478-2764

Complete contact information is available at: https://pubs.acs.org/10.1021/acs.nanolett.0c03189

Notes

The authors declare no competing financial interest.

■ ACKNOWLEDGMENTS

The authors gratefully acknowledge the support of the Stanford Catalyst for Collaborative Solutions under funding ID 132114, the Gates Foundation under OPP 1113682, and the National Science Foundation under grant number 1905209. S.S.G. and H.A. acknowledge partial support from Center for Cancer Nanotechnology Excellence and Translation grant from the NCI-NIH (Grant 1U54CA199075) and the NIH grants (NCI 1R01CA199656-01A1 and 1R01 CA222836-01A1). H.A. acknowledges the support from National Institutes of Health (NIH) K99/R00 Pathway to Independence award (Grant 1K99CA234208-01A1). He was also partly supported by NIH T32 CA009695 Postdoctoral Fellowship (Stanford Cancer Imaging Training, SCIT) program and acknowledges partial support by the Marie Skłodowska-Curie MINDED Project (Grant 754490). Part of this work was performed at the Stanford Nano Shared Facilities (SNSF) and the Soft & Hybrid Materials Facility (SMF), supported by the National Science Foundation under award ECCS-1542152. L.F.T acknowledges support from NIH Biotechnology Training Program under Grant T32GM008412, Agilent, Stanford EDGE and Stanford DARE graduate fellowships. The authors also thank Rich Chin for assistance with SEM imaging and Fareeha Safir, Lisa Poulikakos, and Iwnetim I. Abate for insightful discussions.

■ DEDICATION

This work is dedicated to coauthor Sanjiv Sam Gambhir, who passed away on June 18, 2020; his vision for precision health and early disease diagnostics inspired us and will live on through us.

■ REFERENCES

(1) Caliendo, A. M.; Gilbert, D. N.; Ginocchio, C. C.; Hanson, K. E.; May, L.; Quinn, T. C.; Tenover, F. C.; Alland, D.; Blaschke, A. J.; Bonomo, R. A.; et al. Better tests, better care: improved diagnostics for infectious diseases. *Clin. Infect. Dis.* **2013**, *57* (Suppl 3), S139−70.

(2) Cruz, P.; Mehretu, A. M.; Buttner, M. P.; Trice, T.; Howard, K. M. Development of a polymerase chain reaction assay for the rapid detection of the oral pathogenic bacterium, Selenomonas noxia. *BMC Oral Health* **2015**, *15*, 95.

(3) Singhal, N.; Kumar, M.; Kanaujia, P. K.; Virdi, J. S. MALDI-TOF mass spectrometry: an emerging technology for microbial identification and diagnosis. *Front. Microbiol.* **2015**, *6*, 791.

(4) Schloter, M.; Aßmus, B.; Hartmann, A. The use of immunological methods to detect and identify bacteria in the environment. *Biotechnol. Adv.* **1995**, *13*, 75−90.

(5) Carlsson, H. E.; Lindberg, A. A. Application of Enzyme Immunoassay for Diagnosis of Bacterial and Mycotic Infections. *Scand. J. Immunol.* **1978**, *8*, 97−110.

(6) Li, M.; Xu, J.; Romero-Gonzalez, M.; Banwart, S. A.; Huang, W. E. Single cell Raman spectroscopy for cell sorting and imaging. *Curr. Opin. Biotechnol.* **2012**, *23*, 56−63.

(7) Harz, M.; et al. Micro-Raman spectroscopic identification of bacterial cells of the genus Staphylococcus and dependence on their cultivation conditions. *Analyst* **2005**, *130*, 1543−1550.

(8) Nolan, J. P.; et al. Single cell analysis using surface enhanced Raman scattering (SERS) tags. *Methods* **2012**, *57*, 272−279.

(9) Palonpon, A. F.; et al. Raman and SERS microscopy for molecular imaging of live cells. *Nat. Protoc.* **2013**, *8*, 677−692.

(10) Langer, J.; et al. Present and Future of Surface-Enhanced Raman Scattering. *ACS Nano* **2020**, *14*, 28−117.

(11) Etezadi, D.; et al. Nanoplasmonic mid-infrared biosensor for in vitro protein secondary structure detection. *Light: Sci. Appl.* **2017**, *6*, No. e17029.

(12) Tian, L.; Su, M.; Yu, F.; Xu, Y.; Li, X.; Li, L.; Liu, H.; Tan, W.; et al. Liquid-state quantitative SERS analyzer on self-ordered metal liquid-like plasmonic arrays. *Nat. Commun.* **2018**, *9*, 3642.

(13) Zhang, K.; et al. Large-area graphene nanodot array for plasmon-enhanced infrared spectroscopy. *Small* **2016**, *12*, 1302−1308.

(14) Kumar, G. V. P.; et al. Hot spots in Ag Core−Au shell nanoparticles potent for surface-enhanced Raman scattering studies of biomolecules. *J. Phys. Chem. C* **2007**, *111*, 4388−4392.

(15) Berry, V.; Gole, A.; Kundu, S.; Murphy, C. J.; Saraf, R. F. Deposition of CTAB-terminated nanorods on bacteria to form highly conducting hybrid systems. *J. Am. Chem. Soc.* **2005**, *127*, 17600−17601.

(16) Kuku, G.; Altunbek, M.; Culha, M. Surface-Enhanced Raman Scattering for Label-Free Living Single Cell Analysis. *Anal. Chem.* **2017**, *89*, 11160−11166.

(17) Butler, H. J.; et al. Using Raman spectroscopy to characterize biological materials. *Nat. Protoc.* **2016**, *11*, 664−687.

(18) Zhou, Q.; Kim, T. Review of microfluidic approaches for surface-enhanced Raman scattering. *Sens. Actuators, B* **2016**, *227*, 504−514.

(19) Premasiri, W. R.; et al. The biochemical origins of the surface-enhanced Raman spectra of bacteria: a metabolomics profiling by SERS. *Anal. Bioanal. Chem.* **2016**, *408*, 4631−4647.
(20) Teixeira, A.; et al. Microfluidics-Driven Fabrication of a Low Cost and Ultrasensitive SERS-Based Paper Biosensor. *Appl. Sci.* **2019**, *9*, 1387.
(21) Zhang, X.; Young, M. A.; Lyandres, O.; Van Duyne, R. P. Rapid detection of an anthrax biomarker by surface-enhanced Raman spectroscopy. *J. Am. Chem. Soc.* **2005**, *127*, 4484−4489.
(22) Tadesse, L. F.; et al. Toward rapid infectious disease diagnosis with advances in surface-enhanced Raman spectroscopy. *J. Chem. Phys.* **2020**, *152*, 240902.
(23) Ho, C.-S.; Jean, N.; Hogan, C. A.; Blackmon, L.; Jeffrey, S. S.; Holodniy, M.; Banaei, N.; Saleh, A. A. E.; Ermon, S.; Dionne, J.; et al. Rapid identification of pathogenic bacteria using Raman spectroscopy and deep learning. *Nat. Commun.* **2019**, *10*, 4927.
(24) Boardman, A. K.; et al. Rapid Detection of Bacteria from Blood with Surface-Enhanced Raman Spectroscopy. *Anal. Chem.* **2016**, *88*, 8026−8035.
(25) Zhou, H.; et al. Label-Free in Situ Discrimination of Live and Dead Bacteria by Surface-Enhanced Raman Scattering. *Anal. Chem.* **2015**, *87*, 6553−6561.
(26) Zhou, H.; et al. SERS detection of bacteria in water by in situ coating with Ag nanoparticles. *Anal. Chem.* **2014**, *86*, 1525−1533.
(27) White, I. M.; Yazdi, S. H.; Yu, W. W. Optofluidic SERS: synergizing photonics and microfluidics for chemical and biological analysis. *Microfluid. Nanofluid.* **2012**, *13*, 205−216.
(28) Li, Q.-L.; Li, B.-W.; Wang, Y.-Q. Surface-enhanced Raman scattering microfluidic sensor. *RSC Adv.* **2013**, *3*, 13015−13026.
(29) Walter, A.; März, A.; Schumacher, W.; Rösch, P.; Popp, J. Towards a fast, high specific and reliable discrimination of bacteria on strain level by means of SERS in a microfluidic device. *Lab Chip* **2011**, *11*, 1013−1021.
(30) Zhang, Q.; et al. Towards high-throughput microfluidic Raman-activated cell sorting. *Analyst* **2015**, *140*, 6163−6174.
(31) Song, Y.; Yin, H.; Huang, W. E. Raman activated cell sorting. *Curr. Opin. Chem. Biol.* **2016**, *33*, 1−8.
(32) Jahn, I. J.; et al. Surface-enhanced Raman spectroscopy and microfluidic platforms: challenges, solutions and potential applications. *Analyst* **2017**, *142*, 1022−1047.
(33) Zhang, P.; et al. Raman-activated cell sorting based on dielectrophoretic single-cell trap and release. *Anal. Chem.* **2015**, *87*, 2282−2289.
(34) Ye, X.; Zheng, C.; Chen, J.; Gao, Y.; Murray, C. B. Using binary surfactant mixtures to simultaneously improve the dimensional tunability and monodispersity in the seeded growth of gold nanorods. *Nano Lett.* **2013**, *13*, 765−771.
(35) Van Dijk, T.; et al. Competition Between Extinction and Enhancement in Surface-Enhanced Raman Spectroscopy. *J. Phys. Chem. Lett.* **2013**, *4*, 1193−1196.
(36) Sivapalan, S. T.; et al. Off-resonance surface-enhanced Raman spectroscopy from gold nanorod suspensions as a function of aspect ratio: not what we thought. *ACS Nano* **2013**, *7*, 2099−2105.
(37) Tyers, M.; Wright, G. D. Drug combinations: a strategy to extend the life of antibiotics in the 21st century. *Nat. Rev. Microbiol.* **2019**, *17*, 141−155.
(38) Münchberg, U.; Rösch, P.; Bauer, M.; Popp, J. Raman spectroscopic identification of single bacterial cells under antibiotic influence. *Anal. Bioanal. Chem.* **2014**, *406*, 3041−3050.
(39) De Marchi, S.; et al. Surface-enhanced Raman scattering (SERS) imaging of bioactive metabolites in mixed bacterial populations. *Applied Materials Today* **2019**, *14*, 207−215.
(40) Zhang, Z.; et al. A live bacteria SERS platform for the in situ monitoring of nitric oxide release from a single MRSA. *Chem. Commun.* **2018**, *54*, 7022−7025.

https://dx.doi.org/10.1021/acs.nanolett.0c03189
Nano Lett. 2020, 20, 7655−7661